



Nanoscale

**Gaussian Approximation Potentials for Accurate Thermal Properties of Two-Dimensional Materials**

Journal:	<i>Nanoscale</i>
Manuscript ID	NR-ART-01-2023-000399.R1
Article Type:	Paper
Date Submitted by the Author:	30-Mar-2023
Complete List of Authors:	Kocabas, Tugbey; Eskisehir Teknik Universitesi, Materials Science and Engineering Keçeli, Murat; Argonne National Laboratory, Computational Science Division Vázquez-Mayagoitia, Álvaro; Argonne National Laboratory, Computational Science Division Sevik, Cem; Eskisehir Teknik Universitesi, Mechanical Engineering

SCHOLARONE™  
Manuscripts

# Gaussian Approximation Potentials for Accurate Thermal Properties of Two-Dimensional Materials

Tuğbey Kocabaş,<sup>\*,†</sup> Murat Keçeli,<sup>\*,‡</sup> Álvaro Vázquez-Mayagoitia,<sup>\*,‡</sup> and Cem Sevik<sup>\*,¶,§</sup>

<sup>†</sup>*Department of Materials Science and Engineering, Institute of Graduate Programs, Eskişehir Technical University, Eskişehir TR 26555, Türkiye*

<sup>‡</sup>*Computational Science Division, Argonne National Laboratory, Lemont IL 60517, USA*

<sup>¶</sup>*Department of Physics & NANOlaboratory Center of Excellence, University of Antwerp, Groenenborgerlaan 171, B-2020 Antwerp, Belgium*

<sup>§</sup>*Department of Mechanical Engineering, Eskişehir Technical University, Eskişehir TR 26555, Türkiye*

E-mail: tkocabas@eskisehir.edu.tr; keceli@anl.gov; vama@alcf.anl.gov; csevik@eskisehir.edu.tr

## Abstract

Two-dimensional materials (2DMs) continue to attract a lot of attention, particularly for their extreme flexibility and superior thermal properties. Molecular dynamics simulations are among the most powerful methods for computing these properties, but their reliability depends on the accuracy of interatomic interactions. While first principles approaches provide the most accurate description of interatomic forces, they are computationally expensive. In contrast, classical force fields are computationally efficient, but have limited accuracy in interatomic force description. Machine learning

interatomic potentials, such as Gaussian Approximation Potentials, trained on density functional theory (DFT) calculations offer a compromise by providing both accurate estimation and computational efficiency. In this work, we present a systematic procedure to develop Gaussian approximation potentials for selected 2DMs, graphene, buckled silicene, and  $h$ -XN ( $X = \text{B}, \text{Al}, \text{and Ga}$ , as binary compounds) structures. We validate our approach through calculations that require various levels of accuracy in interatomic interactions. The calculated phonon dispersion curves and lattice thermal conductivity, obtained through harmonic and anharmonic force constants (including fourth order) are in excellent agreement with DFT results. HIPHIVE calculations, in which the generated GAP potentials were used to compute higher-order force constants instead of DFT, demonstrated the first-principles level accuracy of the potentials for interatomic force description. Molecular dynamics simulations based on phonon density of states calculations, which agree closely with DFT-based calculations, also show the success of the generated potentials in high-temperature simulations.

## Introduction

Accurate calculation of interatomic forces is critical for estimating reliable thermal and thermodynamic properties of crystalline and amorphous materials through large-scale molecular dynamics simulations. First-principles methods based on density functional theory (DFT) offer the most reliable approaches for calculating interatomic interactions, but the increased computational cost has been a limiting factor that hinders the study of realistic systems with defects and anharmonicity at scale.<sup>1</sup> An alternative approach, classical force fields (FFs) constructed with parameterized functions, is a computationally efficient solution, but its accuracy in evaluating interatomic forces is limited compared to DFT.<sup>2</sup>

To address the challenge of studying realistic systems with high accuracy and reasonable computational cost, emerging techniques such as machine learning (ML) have gained widespread adoption in the materials science community in the last ten years.<sup>3,4</sup> ML-based

interatomic potentials (MLIPs) offer the potential to achieve a desired level of accuracy at orders of magnitude lower computational cost compared to *ab initio* molecular dynamics (AIMD).<sup>4</sup> One key difference between MLIPs and FFs is the functional form used to represent the interaction potential. While FFs have a fixed functional form, MLIPs do not make assumptions about the form of the potential, except for some physical constraints such as smoothness of the function and a cutoff distance for interactions. This flexible functional form allows MLIPs to achieve the accuracy of the calculations used for training within an arbitrary error. However, the evaluation of forces from MLIPs can be more computationally expensive than FFs due to the complexity of the model, but this cost is still orders of magnitude lower than *ab initio* calculations.<sup>5,6</sup> In addition, the computational cost of MLIPs (which depends on the ML model) generally scales linearly with system size, in contrast to the cubic or higher-order scaling of DFT methods.

The development of accurate MLIPs for various materials is critical for extending the capabilities of these potentials to address thermal and thermodynamic properties of large-scale systems. Several MLIPs such as Gaussian Approximation Potentials (GAP),<sup>5,7</sup> Moment Tensor Potentials (MTP),<sup>8</sup> SchNetPack,<sup>9</sup> Spectral Neighbor Analysis Potential (SNAP),<sup>10</sup> and Neuroevolution Machine Learning Potentials (NEP)<sup>11</sup> have been proposed and tested. We refer readers to recent reviews<sup>3,4</sup> for a comprehensive list of developments in this rapidly growing field. In this study, we focus on GAP models, which typically require less data to be trained than neural network potentials, and have good scalability and computational efficiency for large-scale molecular dynamics simulations.<sup>12</sup> In a previous study,<sup>13</sup> we demonstrated that GAP models trained with DFT calculations<sup>14</sup> provide accurate estimates of the thermal expansion properties of graphene, along with the dominant effect of the rippling/buckling on negative thermal expansion.<sup>15</sup> Other studies have also shown the success of GAP models for thermal properties of 2DMs, such as graphene,<sup>16</sup> carbon allotropes,<sup>17</sup> monolayer *h*-BN,<sup>18</sup> *h*-BN allotropes,<sup>19</sup> silicene,<sup>11,20</sup> and monolayer MoS<sub>2</sub>.<sup>21</sup>

In this work, we propose a streamlined procedure for generating highly accurate GAP

models for 2DMs. We demonstrate our approach for graphene, silicene (as a buckled 2DM), and  $h$ -XN ( $X = \text{B}, \text{Al}, \text{and Ga}$ , as binary 2DMs). In addition to traditional validation using randomly selected data points (excluded from the training set) from *ab initio* molecular dynamics (AIMD) trajectories, we also use thermal property calculations to validate the accuracy of the MLIPs. The first test is the phonon dispersion curves, which provide information about dynamical stability and two-phonon interactions through 2<sup>nd</sup> order interatomic force constants (IFCs). The second test is the iterative solution of lattice thermal conductivity, which also depends on 3<sup>rd</sup> order IFCs and provides information about the anharmonicity of the structure. The accuracy of force prediction for 2<sup>nd</sup> and 3<sup>rd</sup> order force constant calculations is also tested by implementing the HIPHIVE package.<sup>22</sup> The HIPHIVE package is a Python library that aims to generate high-order IFCs with reduced number of force calculations by using advanced optimization and machine learning techniques. Therefore, reference forces (i.e., training data) must be calculated with high (first principles level) accuracy to obtain a reliable output. Finally, the performance of large-scale simulations is confirmed via phonon density of states computed with velocity auto-correlation calculations based on molecular dynamics simulations.

## Methods

Our workflow for developing GAP models and calculating thermal properties is depicted in Figure 1. The procedure for calculating thermal properties of 2D materials is similar to our earlier studies<sup>23,24</sup> as shown on the right side of Figure 1. The key difference here is that we use the thermal property calculations to tune the hyperparameters of MLIP training and to validate the accuracy of the generated potentials.

Density functional theory (DFT) with the Perdew-Burke-Ernzerhof (PBE) generalized gradient approximation (GGA)<sup>25</sup> was used as implemented in the VASP code<sup>26</sup> for relaxing structures and calculating forces on atoms. A plane-wave energy cutoff of 600 eV was adopted

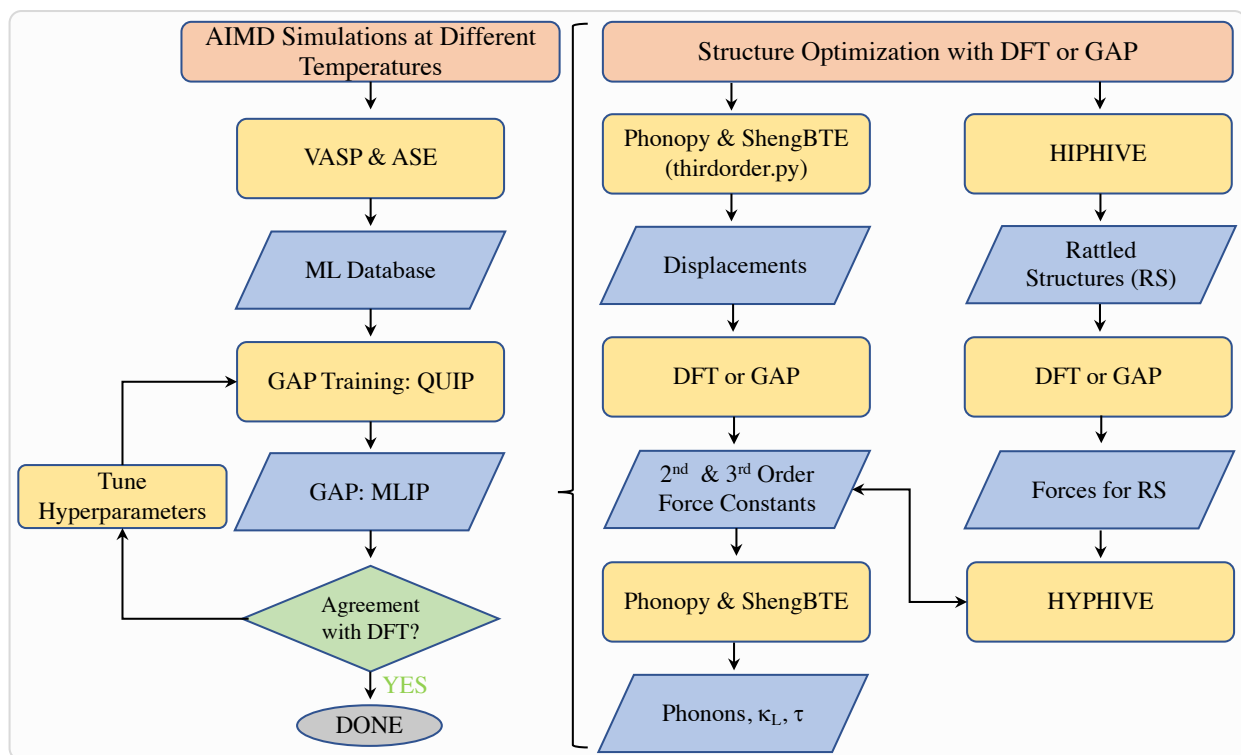


Figure 1: Flowchart illustrating the process for generating and evaluating Gaussian approximation potentials.

in these calculations. The Brillouin-zone integrations were performed using a  $\Gamma$ -centered regular  $24 \times 24 \times 1$   $k$ -point mesh within the Monkhorst-Pack scheme.<sup>27</sup> The convergence criteria for electronic and ionic relaxations were set to  $10^{-6}$  eV and  $10^{-2}$  eV/Å, respectively. A vacuum layer of at least 15 Å along the  $z$ -direction was chosen to avoid interactions between neighbouring layers.

The 2<sup>nd</sup> and 3<sup>rd</sup> order interatomic force constants (IFCs) were calculated with the finite displacement method as implemented in the VASP, Phonopy,<sup>28</sup> and `thirdorder.py`<sup>29</sup> codes. An  $8 \times 8 \times 1$  supercell and a  $3 \times 3 \times 1$   $\Gamma$ -centered  $k$ -points grid were employed, and the total energy convergence limit was set to  $10^{-8}$  eV for electronic minimization to obtain accurate IFCs. IFC calculations based on GAP were performed using the QUIP,<sup>30</sup> quippy Python interface,<sup>31</sup> and Atomic Simulation Environment (ASE)<sup>32</sup> software packages.

AIMD simulations were performed on  $8 \times 8 \times 1$  supercell and  $2 \times 2 \times 1$   $\Gamma$ -centered  $k$ -points grid with a time step of 1 and 3 fs within the NPT ensemble (constant particle, pressure, and temperature)<sup>33</sup> at different temperatures from 200 K to 2000 K. The convergence criteria to calculate energies for DFT calculations is  $10^{-6}$  eV for each step. Different temperatures in AIMD simulations enable us to have diverse structures that correspond to each phonon mode. On the other hand, to avoid overfitting, none of the supercell structures from 2<sup>nd</sup> and 3<sup>rd</sup> order IFCs mentioned in the previous subsection were used in the training datasets.

Lattice thermal conductivity and various thermal transport properties such as phonon lifetimes and Grüneisen parameters, were calculated by iterative solutions of the Peierls-Boltzmann transport equation (PBTE)<sup>34</sup> as implemented in the ShengBTE code.<sup>35</sup> We note the importance of 3<sup>rd</sup> order IFCs for these properties. In lattice thermal transport calculations, at least  $64 \times 64 \times 1$  well converged  $q$ -grid were used and up to 11 next-nearest-neighbour interactions were selected. The out-of-plane lattice constants (layer thickness) were set as 3.35 Å, 4.20 Å, 3.33 Å, 3.40 Å, and 3.49 Å for graphene, silicene,  $h$ -BN,  $h$ -AlN, and  $h$ -GaN respectively.

Phonon density of states (PDOS) is generally calculated by using 2<sup>nd</sup> order IFCs with

*ab-initio* methods. Alternatively, the Fourier transform of velocity autocorrelation function (VACF),  $C_{vv}$ , obtained as a result of MD simulations can be used to calculate PDOS as follows,

$$C_{vv}(t) = \frac{1}{N} \sum_{i=1}^N \frac{\langle \mathbf{v}_i(t) \mathbf{v}_i(0) \rangle}{\langle \mathbf{v}_i(0) \mathbf{v}_i(0) \rangle}, \quad (1)$$

$$D(\omega) = \int_{-\infty}^{\infty} C_{vv}(t) e^{-i\omega t} dt. \quad (2)$$

Here,  $v_i(t)$  corresponds to the velocities of particles along MD trajectories and  $N$  is the number of particles in the simulation box. Finally, PDOS,  $D(\omega)$  can be obtained with the Fourier transform of  $C_{vv}$  as a function of frequency. We used LAMMPS<sup>36</sup> to run MD simulations with the generated MLIPs. The supercell contains 5076 atoms in these simulations and 0.1 fs was used as the time step. Also, 1000 different relative starting points (as  $v(0)$ ) were selected and  $C_{vv}$  values were averaged over 100k steps from that of relative starting points. The stated simulation parameters are at most important to reach accurate values along whole frequency domain.

We generate the training database by running *ab initio* molecular dynamics (AIMD) simulations at different temperatures (T=200 K, 400 K,...) and then randomly selecting points from the trajectories for training and validation. The determination of maximum temperatures in AIMD calculations is based on the phonon frequencies of materials. For instance, the maximum phonon frequency of graphene is around 50 THz, which corresponds to 2400 K; thus, the training database for graphene covers the structures in which outputs of AIMD calculations are from 200 K to 2400 K with 200 K intervals. Since we focus on lattice thermal transport properties using MLIPs, the hyperparameters have been tuned according to the results of the IFCs of the materials. First, phonon dispersion curves, i.e., 2<sup>nd</sup> order, and then thermal conductivity values, i.e., 3<sup>rd</sup> order IFCs have been calculated and compared with DFT results. All the hyperparameters (i.e. the number of training points, cutoff distance, sparse points, etc) were tuned to optimize the computational cost

and accuracy. We found that 3<sup>rd</sup> order IFCs are more sensitive to hyperparameter values compared to 2<sup>nd</sup> order IFCs.

We have used 500 validation points for all the systems while number of training points were between 1500 to 2500 depending on the system. All the values for hyperparameters of each system are given in Table 1. To represent the atomic environment, the smooth overlap of atomic positions<sup>37</sup> (SOAP) descriptor have been chosen. The main reason we use SOAP is its ability to describe both two-body and higher-order many-body interactions in a compact and rotationally invariant fashion. Accurate calculation of forces requires considering surrounding atoms beyond the first neighbors and SOAP particularly works well with mid- and long-range interactions. While we also tested other descriptors and could get good results, using a single descriptor enabled us to develop a more consistent and systematic approach for training.

Table 1: GAP Hyperparameters

Hyperparameters	Graphene	Silicene	<i>h</i> -BN	<i>h</i> -AlN	<i>h</i> -GaN
$l_{max}$	10	12	6	8	6
$n_{max}$	8	10	6	8	8
$r_{cut}$	5.2	7.2	6	5.2	7.2
$\sigma$	0.4	0.5	0.4	0.5	0.4
zeta	4	4	2	4	2
$n_{sparse}$	1500	2000	1000	1000	1500
$\delta$	0.2	0.3	0.2	0.2	0.2

## Results and Discussions

The phonon dispersion relations of 2D materials can provide valuable insights into their stability. On the top row of Figure 2 we present the phonon dispersion curves for graphene, silicene, *h*-BN, *h*-AlN, and *h*-GaN obtained with four different methods: the reference DFT method, the GAP method, the DFT-HIPHIVE method, and GAP-HIPHIVE method. As shown in the figure, the GAP and DFT-HIPHIVE methods are indistinguishable from the DFT results, despite having significantly lower computational costs. Notably, the GAP-

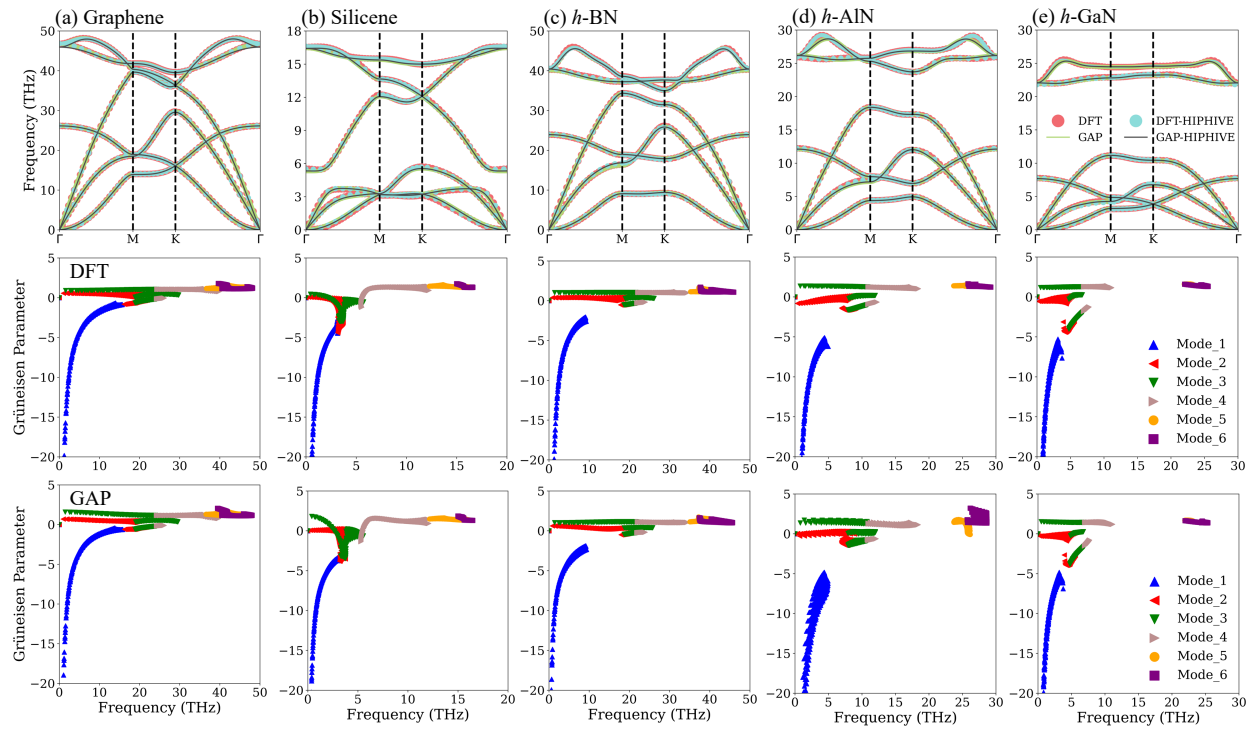


Figure 2: Phonon dispersions (top row) and Grüneisen parameter vs frequency plots with DFT (middle row), and GAP (bottom row) for (a) Graphene, (b) Silicene, (c) *h*-BN, (d) *h*-AlN, and (e) *h*-GaN.

HIPHIVE method, which is based on GAP calculations and therefore has the lowest computational cost, reproduces the phonon dispersion relations closely as well. The middle and bottom rows of Figure 2 present plots of Grüneisen parameters versus frequency for DFT and GAP, respectively, for all the 2D materials. The Grüneisen parameters reflect the derivative of phonon frequencies with respect to crystal volume (or area in the case of 2D systems). While phonon dispersion curves only depend on 2<sup>nd</sup> order force constants, the calculation of Grüneisen parameters requires an accurate description of quasi-harmonic force constants (the first derivatives of frequencies with respect to volume). Therefore, the Grüneisen parameters provide a more stringent test for the accuracy of the GAP models. Our results show that the MLIPs developed in this study are quite successful at predicting quasi-harmonic interactions, with the exception of silicene, where there is an overestimation at low frequencies. In addition, based on the Grüneisen approximation of thermal expansion theory, the generated GAP models yield accurate results for the thermal expansion properties of these materials.

We also calculated the thermal transport properties of these materials using the solution of the phonon Boltzmann transport equation (PBTE) as implemented in the ShengBTE code. By default, this approach requires accurate calculations of ionic forces for 2<sup>nd</sup> and 3<sup>rd</sup> order displacements. The number of structures that must be considered depends on the crystal symmetry and the chosen nearest-neighbour cut-off distance. Therefore, the accuracy, especially for 3<sup>rd</sup> order displacements, is crucial for obtaining an accurate description of the lattice thermal transport properties. Figure 3 a-e compares the thermal transport properties of the 2DMs calculated using both DFT and GAP forces, respectively. Overall, the GAP results for all the 2DMs studied are in good agreement with the reference DFT calculations. In addition, the phonon relaxation times calculated with the consideration of 3<sup>rd</sup> order force constants throughout the Brillouin zone are also consistent with the DFT results. These findings demonstrate the reliability of our GAP models, particularly for thermal calculations. Zhang *et. al*<sup>20</sup> fitted a GAP potential for silicene and predicted its lattice

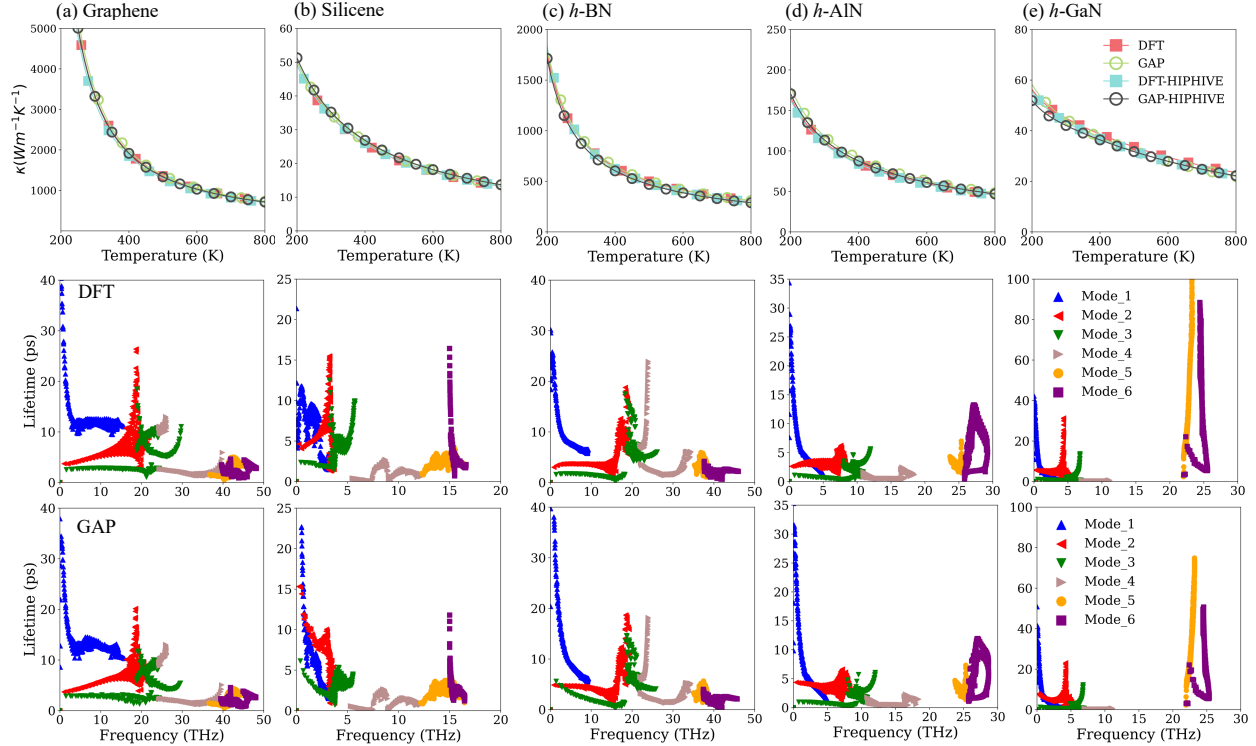


Figure 3: Lattice thermal conductivities. Iterative solution of BTE

thermal conductivity via a sinusoidal approach to equilibrium molecular dynamics (SAEMD) and time domain normal mode analysis (TDNMA) techniques. The calculated room temperature thermal conductivity in our work is in very good agreement with their results. Another GAP potential for silicene, developed and tested for thermal conductivity by Fan *et. al.*<sup>11</sup> also produce nearly the same room temperature thermal conductivity as the one developed in this study. In both previous works, the considered interaction descriptions are more complex due to the inclusion of two-body and three-body interactions in addition to SOAP. Similarly, Quyang *et. al.*<sup>16</sup> adopted the same descriptors for graphene and obtained comparable results with literature in terms of lattice thermal conductivity. The potential generated in our study is as accurate as their potential in that sense. An example application of GAP for lattice thermal conductivity of *h*-BN is also available in the literature,<sup>18</sup> but the training data includes the 3<sup>rd</sup> order displacements, which are intentionally avoided in our study to clearly test the accuracy of developed potentials.

We also compared the DFT and GAP-generated forces using the HIPHIVE code. As shown in the top row of Figure 3, the accuracy of DFT and GAP models in determining 3<sup>rd</sup> order force constants for lattice thermal conductivity calculations is very impressive. Figure S2 in the Supplementary Materials, which presents relaxation time calculations based on HIPHIVE, also supports the accuracy of our potential. It is worth noting that for such good agreement between DFT and HIPHIVE in phonon relaxation time calculations, the forces calculated by GAP-HIPHIVE for the selected set of displacements must be as accurate as the reference DFT calculations. The fact that the generated GAP potentials achieve this level of accuracy and enable the use of an approximate but more efficient method is noteworthy. On the other hand, the  $\kappa$  values reported here are in very good agreement with the values calculated with similar methods and measured experimentally as depicted in Table 2.

Phonon-phonon interactions play a crucial role in determining lattice thermal conductivity in crystals. In first principles-based calculations, these interactions are generally taken into account up to the three-phonon scattering order.<sup>51–55</sup> However, recent studies have highlighted the significant role of higher-order phonon-phonon interactions in accurately determining lattice thermal conductivity, even for graphene.<sup>56–62</sup>

The previous tests for the GAP model were based on static calculations of interatomic forces. To further evaluate the accuracy of the generated potentials in representing physical properties, we performed VACF-based calculations using molecular dynamics trajectories generated by the LAMMPS code. We conducted NVE simulations for all the considered crystals following equilibration NVT simulations using the potentials developed in this study. As shown in the temperature fluctuation data in the Supplementary Materials (Figure S9), the temperature, which is related to the kinetic energy of the particles, is within the limits of accurate molecular dynamics simulations.

The calculated ensemble average phonon density of states, obtained from velocity auto-correlation data using the GAP model, agrees very well with the phonon density of states calculated statically using Phonopy with finite displacement forces calculated by DFT (Fig-

Table 2: The calculated room temperature lattice thermal conductivity of materials in comparison with example calculations and available experimental data. Here, 'EXP', 'HP', 'GK', 'SAEMD', and 'SW' refers to experimental results, HIPHIVE, Green-Kubo, sinusoidal approach-to-equilibrium MD, Stillinger–Weber, respectively.

Material	Approach	$\kappa$ (Wm <sup>-1</sup> K <sup>-1</sup> )	Ref.
Graphene	DFT-BTE	3345	TW
	GAP-BTE	3470	TW
	DFT-HP-BTE	3192	TW
	GAP-HP-BTE	3323	TW
	DFT-BTE	3040	[38]
	MD-GK	2300	[39]
	GAP-BTE	3400	[16]
	EXP	4840-5300	[40]
	EXP	1500-5000	[41]
Silicene	DFT-BTE	34	TW
	GAP-BTE	35	TW
	DFT-HP-BTE	34	TW
	GAP-HP-BTE	35	TW
	DFTB-BTE	34	[42]
	GAP-SAEMD	32	[20]
<i>h</i> -BN	DFT-BTE	915	TW
	GAP-BTE	934	TW
	DFT-HP-BTE	913	TW
	GAP-HP-BTE	873	TW
	DFT-BTE	900	[43]
	DFT-BTE	1242	[44]
	EXP	545	[45]
<i>h</i> -AlN	DFT-BTE	110	TW
	GAP-BTE	118	TW
	DFT-HP-BTE	108	TW
	GAP-HP-BTE	113	TW
	DFT-BTE	73	[46]
	DFT-BTE	78	[43]
	DFT-BTE	70	[47]
<i>h</i> -GaN	DFT-BTE	45	TW
	GAP-BTE	45	TW
	DFT-HP-BTE	43	TW
	GAP-HP-BTE	42	TW
	DFT-BTE	37	[48]
	DFT-BTE	71	[49]
	SW-MD	49	[50]

ure 4). This agreement is particularly impressive when compared with the results obtained using classical force fields.

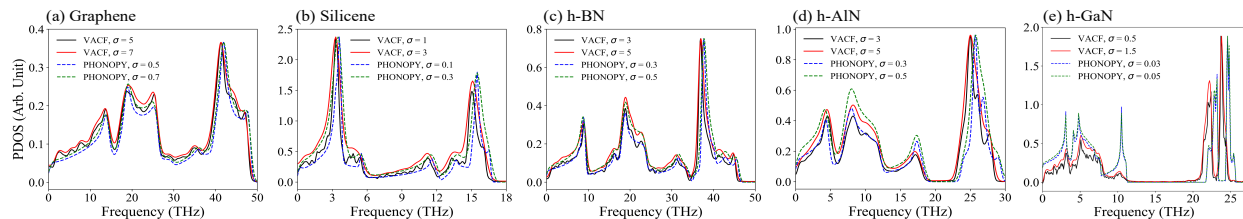


Figure 4: Phonon density of states (PDOS) calculations for (a) Graphene, (b) Silicene, (c) *h*-BN, (d) *h*-AlN, and (e) *h*-GaN.

## Conclusions

In this study, we presented a systematic workflow to generate machine learning potentials for two-dimensional materials. We utilized these potentials to calculate thermoelectric properties of these materials, which requires the computation of higher-order force constants, making it a challenging application for machine learning potentials. We demonstrated that the potentials we trained are as reliable as the reference DFT calculations for thermal property calculations while having orders of magnitude lower computational costs. On average computational time of force calculations with DFT takes approximately 1 hour per structure on a node with 40 cores, while it is only 0.3 seconds on one core with GAP. This speedup allows for longer and larger MD simulations to be run at DFT accuracy. We verified the accuracy of such MD simulations by comparing PDOS calculations with autocorrelation data based on GAP and static Phonopy calculation with DFT. The excellent agreement demonstrates the utility of machine learned potentials is not limited to static properties (i.e., single-step force calculations), and can be reliably used for computing dynamic properties through molecular dynamics simulations. Final GAP models and all the training and validation data were uploaded to a GitHub repository.<sup>63</sup>

## Acknowledgement

Computational resources were provided by the High Performance and Grid Computing Center (TRGrid e Infrastructure) of TUBITAK ULAKBIM and the National Center for High Performance Computing (UHeM) of Istanbul Technical University. We gratefully acknowledge the computing resources provided on Bebop, a high-performance computing cluster operated by the Laboratory Computing Resource Center at Argonne National Laboratory and resources at Argonne Leadership Computing Facility, which is a DOE Office of Science User Facility supported under Contract DE-AC02-06CH11357. M.K. gratefully acknowledges support by Laboratory Directed Research and Development (LDRD) funding from Argonne National Laboratory, provided by the Director, Office of Science, of the U.S. Department of Energy under Contract No.DE-AC02-06CH11357. T.K. thanks the Scientific and Technological Research Council of Türkiye (TUBITAK BİDEB-2211) and the Council of Higher Education of Türkiye (YOK 100/2000) for doctoral scholarship.

## References

- (1) Broido, D. A.; Malorny, M.; Birner, G.; Mingo, N.; Stewart, D. A. Intrinsic lattice thermal conductivity of semiconductors from first principles. *Applied Physics Letters* **2007**, *91*, 67–70.
- (2) Marx, D.; Hutter, J. Ab initio molecular dynamics: Theory and implementation. *Modern methods and algorithms of quantum chemistry* **2000**, *1*, 141.
- (3) Deringer, V. L.; Caro, M. A.; Csányi, G. Machine Learning Interatomic Potentials as Emerging Tools for Materials Science. *Advanced Materials* **2019**, *31*, 1902765.
- (4) Behler, J.; Csányi, G. Machine learning potentials for extended systems: a perspective. *The European Physical Journal B* **2021**, *94*, 142.

- (5) Bartók, A. P.; Payne, M. C.; Kondor, R.; Csányi, G. Gaussian approximation potentials: The accuracy of quantum mechanics, without the electrons. *Physical Review Letters* **2010**, *104*, 136403.
- (6) Behler, J. Perspective: Machine learning potentials for atomistic simulations. *The Journal of chemical physics* **2016**, *145*, 170901.
- (7) Bartók, A. P.; Csányi, G. Gaussian approximation potentials: A brief tutorial introduction. *International Journal of Quantum Chemistry* **2015**, *115*, 1051–1057.
- (8) Novikov, I. S.; Gubaev, K.; Podryabinkin, E. V.; Shapeev, A. V. The MLIP package: moment tensor potentials with MPI and active learning. *Machine Learning: Science and Technology* **2021**, *2*, 025002.
- (9) Schütt, K. T.; Kessel, P.; Gastegger, M.; Nicoli, K. A.; Tkatchenko, A.; Müller, K. R. SchNetPack: A Deep Learning Toolbox for Atomistic Systems. *Journal of Chemical Theory and Computation* **2019**, *15*, 448–455.
- (10) Thompson, A. P.; Swiler, L. P.; Trott, C. R.; Foiles, S. M.; Tucker, G. J. Spectral neighbor analysis method for automated generation of quantum-accurate interatomic potentials. *Journal of Computational Physics* **2015**, *285*, 316–330.
- (11) Fan, Z.; Zeng, Z.; Zhang, C.; Wang, Y.; Song, K.; Dong, H.; Chen, Y.; Ala-Nissila, T. Neuroevolution machine learning potentials: Combining high accuracy and low cost in atomistic simulations and application to heat transport. *Physical Review B* **2021**, *104*, 1–15.
- (12) Zuo, Y.; Chen, C.; Li, X.; Deng, Z.; Chen, Y.; Behler, J.; Csányi, G.; Shapeev, A. V.; Thompson, A. P.; Wood, M. A., et al. Performance and cost assessment of machine learning interatomic potentials. *The Journal of Physical Chemistry A* **2020**, *124*, 731–745.

- (13) Demirođlu, I.; Karaaslan, Y.; Kocabař, T.; Keçeli, M.; Vázquez-Mayagoitia, Á.; Sevıık, C. Computation of the Thermal Expansion Coefficient of Graphene with Gaussian Approximation Potentials. *The Journal of Physical Chemistry C* **2021**, *125*, 14409–14415.
- (14) Rowe, P.; Csányi, G.; Alfè, D.; Michaelides, A. Development of a machine learning potential for graphene. *Physical Review B* **2018**, *97*, 1–12.
- (15) Mondal, S.; Datta, A. Negative Thermal Expansion Induced in Tri-graphene and T-graphene by the Rigid-Unit Modes. *Journal of the American Chemical Society* **2022**, *144*, 16703–16707, PMID: 36069493.
- (16) Ouyang, Y.; Zhang, Z.; Yu, C.; He, J.; Yan, G.; Chen, J. Accuracy of Machine Learning Potential for Predictions of Multiple-Target Physical Properties. *Chinese Physics Letters* **2020**, *37*, 1–9.
- (17) Rowe, P.; Deringer, V. L.; Gasparotto, P.; Csányi, G.; Michaelides, A. An accurate and transferable machine learning potential for carbon. *Journal of Chemical Physics* **2020**, *153*.
- (18) Zhang, Y.; Shen, C.; Long, T.; Zhang, H. Thermal conductivity of h-BN monolayers using machine learning interatomic potential. *Journal of Physics Condensed Matter* **2021**, *33*.
- (19) Thiemann, F. L.; Rowe, P.; Müller, E. A.; Michaelides, A. Machine Learning Potential for Hexagonal Boron Nitride Applied to Thermally and Mechanically Induced Rippling. *Journal of Physical Chemistry C* **2020**, *124*, 22278–22290.
- (20) Zhang, C.; Sun, Q. Gaussian approximation potential for studying the thermal conductivity of silicene. *Journal of Applied Physics* **2019**, *126*.

- (21) Wei, Z.; Zhang, C.; Kan, Y.; Zhang, Y.; Chen, Y. Developing machine learning potential for classical molecular dynamics simulation with superior phonon properties. *Computational Materials Science* **2022**, *202*, 111012.
- (22) Eriksson, F.; Fransson, E.; Erhart, P. The Hiphive Package for the Extraction of High-Order Force Constants by Machine Learning. *Advanced Theory and Simulations* **2019**, *2*, 1800184.
- (23) Kocabaş, T.; Çakır, D.; Gülseren, O.; Ay, F.; Perkgöz, N. K.; Sevik, C. A distinct correlation between the vibrational and thermal transport properties of group VA monolayer crystals. *Nanoscale* **2018**, *10*, 7803–7812.
- (24) Sarikurt, S.; Çakır, D.; Keçeli, M.; Sevik, C. The influence of surface functionalization on thermal transport and thermoelectric properties of MXene monolayers. *Nanoscale* **2018**, *10*, 8859–8868.
- (25) Perdew, J. P.; Burke, K.; Ernzerhof, M. Generalized gradient approximation made simple. *Physical Review Letters* **1996**, *77*, 3865–3868.
- (26) Kresse, G.; Hafner, J. Ab initio molecular dynamics for liquid metals. *Physical Review B* **1993**, *47*, 558–561.
- (27) Monkhorst, H. J.; Pack, J. D. Special points for Brillouin-zone integrations. *Physical Review B* **1976**, *13*, 5188–5192.
- (28) Togo, A.; Tanaka, I. First principles phonon calculations in materials science. *Scripta Materialia* **2015**, *108*, 1–5.
- (29) Li, W.; Lindsay, L.; Broido, D. A.; Stewart, D. A.; Mingo, N. Thermal conductivity of bulk and nanowire Mg<sub>2</sub>Si<sub>x</sub>Sn<sub>1-x</sub> alloys from first principles. *Physical Review B - Condensed Matter and Materials Physics* **2012**, *86*, 174307.

- (30) Csányi, G.; Winfield, S.; Kermode, J. R.; De Vita, A.; Comisso, A.; Bernstein, N.; Payne, M. C. Expressive Programming for Computational Physics in Fortran 95+. *IoP Comput. Phys. Newsletter* **2007**, Spring 2007.
- (31) Kermode, J. R. f90wrap: an automated tool for constructing deep Python interfaces to modern Fortran codes. *J. Phys. Condens. Matter* **2020**, *32*, 305901.
- (32) Larsen, A. H. et al. The atomic simulation environment—a Python library for working with atoms. *Journal of Physics: Condensed Matter* **2017**, *29*, 273002.
- (33) Heyes, D. M. Molecular dynamics at constant pressure and temperature. *Chemical Physics* **1983**, *82*, 285–301.
- (34) Ziman, J. *Electrons and Phonons: The Theory of Transport Phenomena in Solids*; Oxford University Press, 1960.
- (35) Li, W.; Carrete, J.; Katcho, N. A.; Mingo, N. ShengBTE: A solver of the Boltzmann transport equation for phonons. *Computer Physics Communications* **2014**, *185*, 1747–1758.
- (36) Plimpton, S. Fast Parallel Algorithms for Short-Range Molecular Dynamics. *Journal of Computational Physics* **1995**, *117*, 1–19.
- (37) Bartók, A. P.; Kondor, R.; Csányi, G. On representing chemical environments. *Phys. Rev. B* **2013**, *87*, 184115.
- (38) Wang, H.; Qin, G.; Qin, Z.; Li, G.; Wang, Q.; Hu, M. Lone-Pair Electrons Do Not Necessarily Lead to Low Lattice Thermal Conductivity: An Exception of Two-Dimensional Penta-CN2. *Journal of Physical Chemistry Letters* **2018**, *9*, 2474–2483.
- (39) Haskins, J.; Kinaci, A.; Sevik, C.; Sevinçli, H.; Cuniberti, G.; Çağın, T. Control of thermal and electronic transport in defect-engineered graphene nanoribbons. *ACS Nano* **2011**, *5*, 3779–3787.

- (40) Balandin, A. A.; Ghosh, S.; Bao, W.; Calizo, I.; Teweldebrhan, D.; Miao, F.; Lau, C. N. Superior thermal conductivity of single-layer graphene. *Nano Letters* **2008**, *8*, 902–907.
- (41) Jauregui, L. A.; Yue, Y.; Sidorov, A. N.; Hu, J.; Yu, Q.; Lopez, G.; Jalilian, R.; Benjamin, D. K.; Delkd, D. A.; Wu, W., et al. Thermal transport in graphene nanostructures: Experiments and simulations. *Ecs Transactions* **2010**, *28*, 73.
- (42) Wang, Q.; Wang, X.; Guo, R.; Huang, B. Parametrization of density functional tight-binding method for thermal transport in bulk and low-dimensional Si systems. *The Journal of Physical Chemistry C* **2017**, *121*, 15472–15480.
- (43) Kourra, M.; Sadki, K.; Drissi, L.; Bousmina, M. Mechanical response, thermal conductivity and phononic properties of group III-V 2D hexagonal compounds. *Materials Chemistry and Physics* **2021**, *267*, 124685.
- (44) Fan, H.; Wu, H.; Lindsay, L.; Hu, Y. Ab initio investigation of single-layer high thermal conductivity boron compounds. *Physical Review B* **2019**, *100*, 085420.
- (45) Ying, H.; Moore, A.; Cui, J.; Liu, Y.; Li, D.; Han, S.; Yao, Y.; Wang, Z.; Wang, L.; Chen, S. Tailoring the thermal transport properties of monolayer hexagonal boron nitride by grain size engineering. *2D Materials* **2019**, *7*, 015031.
- (46) Wang, H.; Yu, L.; Xu, J.; Wei, D.; Qin, G.; Yao, Y.; Hu, M. Intrinsically low lattice thermal conductivity of monolayer hexagonal aluminum nitride (h-AlN) from first-principles: A comparative study with graphene. *International Journal of Thermal Sciences* **2021**, *162*, 106772.
- (47) Banerjee, A.; Das, B. K.; Chattopadhyay, K. K. Significant enhancement of lattice thermal conductivity of monolayer AlN under bi-axial strain: a first principles study. *Physical Chemistry Chemical Physics* **2022**, *24*, 16065–16074.

- (48) Jiang, Y.; Cai, S.; Tao, Y.; Wei, Z.; Bi, K.; Chen, Y. Phonon transport properties of bulk and monolayer GaN from first-principles calculations. *Computational Materials Science* **2017**, *138*, 419–425.
- (49) Cai, X.; Sun, G.; Xu, Y.; Ma, J.; Xu, D. Effect of hydrogenation on the thermal conductivity of 2D gallium nitride. *Physical Chemistry Chemical Physics* **2021**, *23*, 22423–22429.
- (50) Zhang, J. Piezoelectric effect on the thermal conductivity of monolayer gallium nitride. *Journal of Applied Physics* **2018**, *123*, 035102.
- (51) Esfarjani, K.; Chen, G.; Stokes, H. T. Heat transport in silicon from first-principles calculations. *Phys. Rev. B* **2011**, *84*, 085204.
- (52) Lindsay, L.; Broido, D. A.; Reinecke, T. L. First-Principles Determination of Ultrahigh Thermal Conductivity of Boron Arsenide: A Competitor for Diamond? *Phys. Rev. Lett.* **2013**, *111*, 025901.
- (53) Seko, A.; Togo, A.; Hayashi, H.; Tsuda, K.; Chaput, L.; Tanaka, I. Prediction of Low-Thermal-Conductivity Compounds with First-Principles Anharmonic Lattice-Dynamics Calculations and Bayesian Optimization. *Phys. Rev. Lett.* **2015**, *115*, 205901.
- (54) Lindsay, L.; Hua, C.; Ruan, X.; Lee, S. Survey of ab initio phonon thermal transport. *Materials Today Physics* **2018**, *7*, 106–120.
- (55) McGaughey, A. J. H.; Jain, A.; Kim, H.-Y.; Fu, B. Phonon properties and thermal conductivity from first principles, lattice dynamics, and the Boltzmann transport equation. *Journal of Applied Physics* **2019**, *125*, 011101.
- (56) Feng, T.; Ruan, X. Four-phonon scattering reduces intrinsic thermal conductivity of graphene and the contributions from flexural phonons. *Phys. Rev. B* **2018**, *97*, 045202.

- (57) Yang, X.; Feng, T.; Kang, J. S.; Hu, Y.; Li, J.; Ruan, X. Observation of strong higher-order lattice anharmonicity in Raman and infrared spectra. *Phys. Rev. B* **2020**, *101*, 161202.
- (58) Feng, T.; Ruan, X. Quantum mechanical prediction of four-phonon scattering rates and reduced thermal conductivity of solids. *Phys. Rev. B* **2016**, *93*, 045202.
- (59) Feng, T.; Lindsay, L.; Ruan, X. Four-phonon scattering significantly reduces intrinsic thermal conductivity of solids. *Phys. Rev. B* **2017**, *96*, 161201.
- (60) Xia, Y.; Chan, M. K. Y. Anharmonic stabilization and lattice heat transport in rocksalt  $\beta$ -GeTe. *Applied Physics Letters* **2018**, *113*, 193902.
- (61) Ravichandran, N. K.; Broido, D. Unified first-principles theory of thermal properties of insulators. *Phys. Rev. B* **2018**, *98*, 085205.
- (62) Kundu, A.; Yang, X.; Ma, J.; Feng, T.; Carrete, J.; Ruan, X.; Madsen, G. K. H.; Li, W. Ultrahigh Thermal Conductivity of  $\theta$ -Phase Tantalum Nitride. *Phys. Rev. Lett.* **2021**, *126*, 115901.
- (63) Kocabaş, T.; Keçeli, M.; Vázquez-Mayagoitia, Á.; Sevik, C. GAP models for 2D Materials. 2023; <https://github.com/AI4Materials/2DM-GAP>.